Free Radical Research, September 2007; 41(9): 1005–1016

informa
healthcare

Bicarbonate and active site zinc modulate the self-peroxidation of bovine copper-zinc superoxide dismutase

MICHAEL R. GUNTHER & JOSEPH A. DONAHUE

Department of Biochemistry and Molecular Pharmacology, West Virginia University School of Medicine, Morgantown, WV, USA

Accepted by Professor N. Taniguchi

(Received 13 November 2006; in revised form 15 June 2006)

Abstract
Peroxidation reactions of copper-zinc superoxide dismutase (CuZn-SOD1) or its zinc-depleted form (CuE-SOD1) that likely also involve a component of bicarbonate buffer have been implicated in the pathophysiology of the neurodegenerative diseases amyotrophic lateral sclerosis (ALS), Alzheimer's Disease and Parkinson's Disease. Neither removal of the zinc ion nor adding bicarbonate had large effects on the self-peroxidation reaction of bovine SOD1, but the combination of zinc-deficiency and added bicarbonate caused major changes to the spin trapped SOD1-centred free radical. Removal of the active site zinc ion greatly decreased the formation of an unassigned SOD1-centred free radical in the reaction with the inorganic peroxide peroxynitrite. The results suggest that under cellular conditions ($\sim$5 mM bicarbonate) zinc-deficient SOD1 peroxidation could play a pathogenic role in neurodegenerative diseases.

Keywords: *Superoxide dismutase, hydrogen peroxide, free radical, MNP, zinc, amyotrophic lateral sclerosis*

Introduction

Reactions in which copper-zinc superoxide dismutase (SOD1) oxidizes substrates or is itself oxidized have been implicated in the pathophysiology of amyotrophic lateral sclerosis (ALS) [1–11], Alzheimer's Disease [12] and Parkinson's Disease [12]. Excessive and improper oxidant production by point mutant SOD1 proteins has been suggested to play a significant role in their selective motor neuron toxicity [4–11]. Increased cellular oxidations have also been strongly implicated along the pathophysiological pathways of Alzheimer's disease [13] and Parkinson's disease [14]. The recently detected increased levels of oxidized SOD1 proteins in brains from Alzheimer's disease and Parkinson's disease patients accompanied by SOD1 isoform shifts of unknown aetiology in the patients [12] strongly suggest a role for reactions between the SOD1 protein and oxidants such as H_2O_2 in those diseases. Furthermore, abundant experimental data support a role for H_2O_2 in the pathophysiology of each of the above neurodegenerative diseases [10,11,14–16].

Because expression of mutant forms of the SOD1 protein has been clearly shown to cause ALS [1–3], numerous studies of the physical properties of the mutant proteins have been reported [17–23]. In general, the mutant SOD1 proteins are less stable than the wild type SOD1 protein [17–19] and have a greatly increased tendency to form macromolecular aggregates [24–26] which may or may not contribute to the neurotoxicity of the mutant proteins [27]. Another property that appears to be shared by the mutant SOD1 proteins is a decreased affinity for the structural active site zinc ion [20–23]. Furthermore, treatment of cultured neuronal cells

Correspondence: Michael R. Gunther, PhD, Department of Biochemistry and Molecular Pharmacology, West Virginia University, PO Box 9142, Morgantown, WV 26506, USA. Tel: 304 293 0714. Fax: 304 293 6846. E-mail: mgunther@hsc.wvu.edu

ISSN 1071-5762 print/ISSN 1029-2470 online
DOI: 10.1080/10715760701516308

with zinc-depleted SOD1 proteins, either wild type or mutant, has been clearly shown to contribute to death of the motor neurons [23].

Previously reported data has supported inactivation of the SOD1 protein and, in the presence of bicarbonate, formation of a highly oxidizing carbonate radical anion when native SOD1 proteins react with H_2O_2 [28–41]. The SOD1-H_2O_2 reaction involves multiple steps, starting with the reduction of the active site copper (the SOD1 back reaction) followed by oxidant formation (see reactions 1–5) [34,41]. The initial oxidant formed has similar reactivity to hydroxyl radical but does not appear to leave the active site (reaction 2).

$$\text{SOD1-Cu}^{2+} + \text{H}_2\text{O}_2 \rightarrow \text{SOD1-Cu}^{+} + \text{HO}_2\bullet + \text{H}+ \quad (1)$$

$$\text{SOD1-Cu}^{+} + \text{H}_2\text{O}_2 \rightarrow \text{SOD1-Cu}^{2+}(\text{HO}\bullet) + \text{H}_2\text{O} \quad (2)$$

$$\text{SOD1-Cu}^{2+}(\text{HO}\bullet) \rightarrow \text{SOD1-inactive} + \text{H}_2\text{O} \quad (3)$$

$$\text{SOD1-Cu}^{2+}(\text{HO}\bullet) + \text{(bi)carbonate} \rightarrow \text{SOD1-Cu}^{2+} + \text{CO}_3\bullet^- + \text{H}_2\text{O} \quad (4)$$

$$\text{CO}_3\bullet^- + \text{Substrate} \rightarrow \text{S}\bullet + \text{HCO}_3^- \quad (5)$$

However, the reactions between the zinc-deficient (CuE-) form of the protein with H_2O_2 have not been carefully characterized. To answer that question, we have studied the self-peroxidation reactions of bovine CuZn- and CuE-SOD1 proteins, determining the initial products.

Methods

Materials

Purified bovine SOD1 and Pronase were from Roche Molecular Biopharmaceuticals (Indianapolis, IN). Hydrogen peroxide (30%) was from Fisher (Pittsburgh, PA). Tetramethylammonium peroxynitrite was from A.G. Scientific (San Diego, CA). The spin trap 2-methyl-2-nitrosopropane was from Aldrich Chemical Company (Milwaukee, WI), as was diethylenetriaminepentaacetic acid (DTPA). 3,5-dibromo-4-nitrosobenzenesulphonic acid (DBNBS) was a gift from Mr Bob Sik at the National Institute of Environmental Health Sciences (Research Triangle Park, NC).

Preparation of zinc-depleted SOD1 protein

Zinc-depleted bovine SOD1 protein was prepared following the procedure previously reported by Sampson and Beckman [42]. Briefly, bovine SOD1 protein was dialysed against two charges of Chelex-treated 100 mM potassium phosphate buffer, pH 3.5 and overnight against two charges of Chelex-treated 5 mM sodium acetate buffer, pH 4.2. After a 2-h treatment with copper sulphate (110% of expected sub-unit concentration based on the amount of SOD1 protein used) the protein was again dialysed overnight against 5 mM sodium acetate buffer, pH 4.2. The copper and zinc contents of the resulting SOD1 solutions were determined either by atomic absorbance spectroscopy using a Perkin-Elmer 380 Atomic Absorbance spectrophotometer or spectrophotometrically using the pyridylazaresorcinol assay described by Crow et al. [20]. Protein concentrations were determined using the BCA protein assay from Pierce Chemical Company using bovine serum albumin as a standard.

Electron Paramagnetic Resonance (EPR) spectroscopy

EPR spectra were obtained using a Bruker EMX EPR spectrometer equipped with a Bruker ER4119 HS resonator. Samples (150 µl total volume) were prepared in 1.5 ml plastic centrifuge tubes and were transferred to a quartz flat cell (Wilmad Glass Co, Buena, NJ) before spectra were obtained. Simulations of EPR spectra were performed using the WinSim program and the Powfit program of the NIEHS Public ESR Software Tools package available from the National Institute of Environmental Health Sciences (http://www.epr.niehs.nih.gov/). Optimized EPR spectral simulations were obtained allowing the computer programs to systematically adjust all of the spectral parameters to obtain the best mathematical fit to the experimental data.

Nitrotyrosine determinations

The nitrotyrosine content of SOD1 samples treated with tetramethylammonium peroxynitrite was determined from the absorbance spectrum of those samples [43]. SOD1 samples treated with peroxynitrite were diluted into 50 mM sodium phosphate buffer, pH 7.4 and the absorbance spectrum of those samples from 350–500 nm was determined using an Aminco DW2000 spectrophotometer equipped with computerized data acquisition software. The nitrotyrosine concentration was calculated from the absorbance at 425 nm using an extinction coefficient of 4400 M/cm [43].

Results

The reaction between CuE-SOD1 and H_2O_2 produces active site histidinyl radicals

We hypothesized that the absence of the structural zinc ion would cause the detection of a SOD1-centred radical distinct from the histidinyl radical we previously reported [41]. However, the MNP adducts formed in the H_2O_2 reactions of CuZn-SOD1 and CuE-SOD1 had EPR spectra that were essentially indistinguishable (Figures 1A and F). Cleavage of the protein MNP-adducts into peptides *via* Pronase-treatment resulted in the conversion of their anisotropic EPR spectra into isotropic spectra with complicated hyperfine coupling patterns (Figures 1B and G). Inspection of the spectra

obtained from the Pronase-treated samples suggested trapping at an atom with one bond to a nitrogen ($I = 1$, $a^N = 0.25$ mT) and one bond to a hydrogen atom ($I = ½$, $a^H = 0.11$ mT). Those hyperfine data combined with the $a^{N(NO)}$ of 1.52 mT (matching the previously described value for a MNP/•histidine adduct [41]) were consistent with trapping at C-5 of a histidine imidazole ring. Although the line positions were well fit by a simulation using those parameters, inclusion of an additional species (50% of the total intensity) with hyperfine couplings to two nearly equivalent nitrogens and an additional hydrogen nucleus (hyperfine splitting constants are in Table I), consistent with the C-2-centred histidinyl radical [41], was required to adequately fit the line intensities and shapes of the spec-

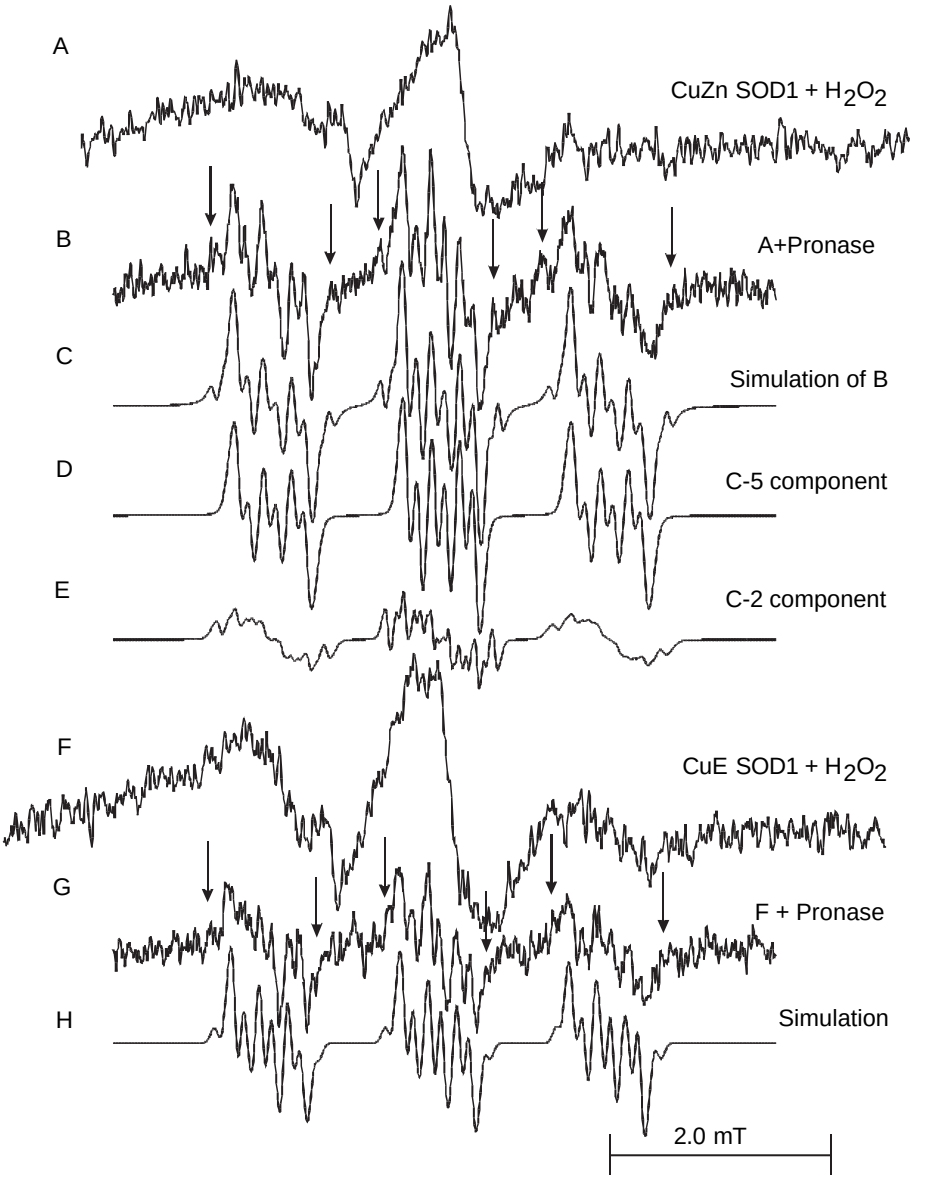

Figure 1. Histidinyl radical formation from the reaction of CuZn SOD1 or CuE SOD1 with H_2O_2 in phosphate buffer. In all cases, SOD1 (0.5 mM copper) was incubated with MNP (10 mM), DTPA (1 mM) and H_2O_2 (2.5 mM) at room temperature. (A) CuZn SOD1 + H_2O_2 + MNP. (B) The same as Spectrum A after a 5-min incubation at room temperature with Pronase (10 mg/ml). The arrows indicate lines in the spectrum arising from the radical adduct assigned to C-2 of the imidazole ring of histidine. (C) Composite simulation of Spectrum B including a 50:50 mixture of two different components with the hyperfine coupling constants indicated in Table I. (D) The first component of the computer simulation of Spectrum B. (E) The second component of the computer simulation of Spectrum B. (F) The EPR spectrum obtained after incubation of CuE SOD1 with MNP and H_2O_2 for 5 min at room temperature. (G) The EPR spectrum obtained after incubation of a solution identical to the solution giving rise to Spectrum F with Pronase (10 mg/ml) for 5 min at room temperature. (H) Computer simulation of Spectrum G calculated using a 50:50 mix of the same components as used in Spectrum C; the hyperfine coupling constants used for the simulation are indicated in Table I. Experimental spectra A and F were acquired using the following instrument parameters: modulation amplitude, 2 G; scan time 335 s (8.0 mT scan); time constant, 0.66 s.; three scans were averaged together to obtain the spectra. Experimental spectra B and G were obtained using the following instrument parameters: modulation amplitude, 1 G; scan time 335 s (6.0 mT scan); time constant, 0.66 s; 20 scans were added together to obtain the final spectra.

Table I. Hyperfine coupling constants from EPR spectral simulations.

Sample	$a^{N(NO)}$(mT)	$a^{N\beta 1}$(mT)	$a^{N\beta 2}$(mT)	a^{H1}(mT)	a^{H2}(mT)	% of total
CuZn/MNP/H_2O_2 (1)	1.52	0.253	N/A	0.11	N/A	50
CuZn/MNP/H_2O_2 (2)	1.53	0.16	0.16	0.18	0.085	50
CuE/MNP/H_2O_2 (1)	1.52	0.25	N/A	0.11	N/A	50
CuE/MNP/H_2O_2 (2)	1.53	0.16	0.16	0.18	0.09	50
CuZn/MNP/HCO_3^-/H_2O_2	1.53	0.26	N/A	0.11	N/A	100
CuE/MNP/HCO_3^-/H_2O_2	1.49	0.243	N/A	N/A	N/A	100
CuZn/MNP/$ONOO^-$	1.60	N/A	N/A	0.11 (2)	N/A	100
CuE/DBNBS/H_2O_2	1.37	0.09	0.07	N/A	N/A	100
CuE/DBNBS/H_2O_2/HCO_3^-	1.35	0.09	0.06	N/A	N/A	100
Histidine/DBNBS (1)	1.34	0.08	0.06	N/A	N/A	49
Histidine/DBNBS (2)	1.36	0.36	N/A	0.72	N/A	51

All values were determined from simulations calculated using the WinSim program from NIEHS. Simulations were optimized allowing the program to select the final values of the hyperfine coupling constants and linewidths to minimize the sum of the residual. Numbers indicated in parentheses indicate the number of identical nuclei with the indicated hyperfine coupling constant.

trum (Figure 1C). Those results indicate either trapping at two separate histidine residues or at two separate sites on the same histidine residue, but the two possibilities cannot be distinguished from the data.

(Bi)carbonate has subtle effects upon the self-peroxidation reaction of CuZn-SOD1

A component of the bicarbonate buffer system (either HCO_3^- or CO_2 (aq), designated '(bi)carbonate') has been reported to be essential for SOD1-mediated substrate oxidations [33–40]. We were therefore interested in the potential role of the same molecule on the self-peroxidation reaction of SOD1. The MNP-radical adduct formed in the reaction between CuZn-SOD1 and H_2O_2 in buffer containing 25 mM bicarbonate had an EPR spectrum that was highly similar to that of the adduct obtained in the absence of added bicarbonate (compare Figures 2A and 1A), confirmed by the difference spectrum obtained by subtracting Figure 1A from Figure 2A (Figure 2B). The spectrum obtained after Pronase-treatment (Figure 2C) was adequately simulated using only the imidazole C-5-centred adduct discussed above (Figure 2D). Those results suggested that, in CuZn-SOD1, the inclusion of (bi)carbonate affected only which histidine residue was oxidized, rather than causing the oxidation of additional site(s) on the protein.

Inclusion of (bi)carbonate changes the major free radical product of the peroxide-CuE-SOD1 reaction

The EPR spectrum obtained from a mixture of CuE-SOD1, (bi)carbonate, MNP and H_2O_2 (Figure 2E) had a significantly increased intensity and a different lineshape compared to the spectrum obtained from MNP/•CuE-SOD1 without (bi)carbonate (Figure 1F). Subtraction of spectrum 1F from spectrum 2E resulted in a difference EPR spectrum (Figure 2F) that was shifted toward a lower magnetic field (corresponding to a higher g-value) and was significantly narrower than the other rotationally immobilized nitroxide EPR spectra. However, the majority of the MNP adduct obtained from CuE-SOD1/H_2O_2/(bi)carbonate was unstable to Pronase-treatment (Figure 2G), precluding its assignment from an isotropic EPR spectrum.

The major MNP/•CuE-SOD1/(bi)carbonate adduct is centred on a carbonyl carbon

The EPR spectra of protein-centred MNP radical adducts are typically anisotropic due to steric hindrance to free rotation of the nitroxide free radical. We therefore simulated the anisotropic EPR spectra obtained from the MNP/•CuZn-SOD1 and MNP/•CuE-SOD1 adducts as powder pattern EPR spectra in order to obtain approximate isotropic g-values and nitroxide nitrogen hyperfine coupling constants from those spectra (Figure 3). As shown in Figure 3A, the anisotropic EPR spectrum obtained from CuZn-SOD1 could be adequately simulated as a powder pattern EPR spectrum using parameters corresponding to an isotropic g-value of $\sim$2.0044 and an isotropic a^N of $\sim$1.51 mT (parameters are reported in the legend of Figure 3). The spectra obtained from MNP/•CuZn-SOD1 + (bi)carbonate and from MNP/•CuE-SOD1 could also be adequately simulated with parameters that gave the same approximate g-value and nitroxide hyperfine coupling constant (Figure 3B and C). The spectrum obtained from MNP/•CuE-SOD1 + (bi)carbonate was not adequately fit with those parameters. To obtain a good fit to the experimental spectrum, two components were used, the first (8% of total intensity) similar to the parameters used for the prior spectra and the second (92% of total intensity) with parameters that provided an approximate isotropic g-value of 2.0053 and an approximate a^N_{iso} of 0.8 mT (Figure 3D). Inclusion

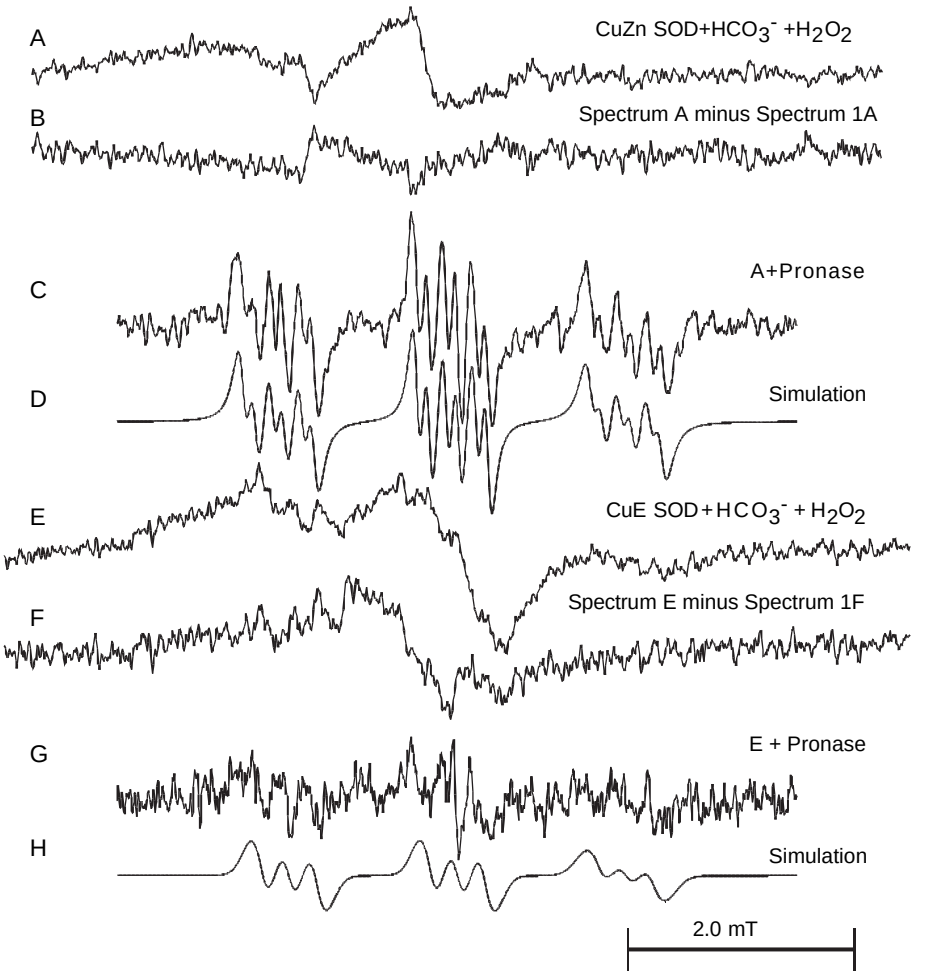

Figure 2. The free radical trapped by MNP in the reaction between CuE-SOD1 and H_2O_2 is altered by bicarbonate buffer. Bovine SOD1 (0.5 mM) was incubated with MNP (10 mM), DTPA (1 mM) and H_2O_2 (2.5 mM) in bicarbonate buffer (25 mM, pH 7.4) for 5 min at room temperature before the EPR spectra were obtained. (A) The EPR spectrum obtained from an incubation of CuZn SOD1, H_2O_2 and MNP. (B) The difference spectrum obtained by subtracting the spectrum shown in Figure 1A from Spectrum 2A. (C) The EPR spectrum obtained after incubation of a sample identical to the one used to obtain Spectrum A with Pronase (10 mg/ml) for 5 min at room temperature. (D) The computer simulation of Spectrum 2C calculated using the hyperfine coupling constants reported in Table I. Inclusion of a second component (the component assigned to trapping histidinyl radical at C-2 in Figure 1) at 10% of the total intensity did not improve the fit of the simulated spectrum to the experimental spectrum. (E) The EPR spectrum obtained from a solution containing CuE SOD1, MNP, DTPA and H_2O_2. (F) The difference spectrum obtained from the subtraction of the spectrum in Figure 1F from Spectrum 2E. (G) The EPR spectrum obtained after incubation of a solution identical to the solution giving rise to Spectrum E after a 5-min incubation with Pronase (10 mg/ml). (H) Computer simulation of Spectrum 2G calculated using the hyperfine coupling constants reported in Table I. The experimental spectra were obtained using the same instrument parameters as reported in Figure 1.

of ~9% of the latter adduct in the simulation of the MNP/•CuZn-SOD1 + (bi)carbonate spectrum slightly improved the fit of the simulation to the experimental spectrum (Figure 3B). MNP adducts with a^N of ~0.8 mT have been previously reported from carbonyl carbon-centred radical adducts obtained by oxidizing the carboxylate groups of amino acids by persulphate radical [44], oxidation of acetylacetone by horseradish peroxidase and H_2O_2 [45] and from oxidizing N,N-dimethylamides [46]. The amino acid adducts reported in Rustgi and Riesz [44] were highly unstable and could only be observed in a flow experiment, as was the (bi)carbonate-dependent MNP/•CuE-SOD1 adduct.

The second free radical product of the CuE-SOD1/H_2O_2/(bi)carbonate reaction is a histidinyl radical

The EPR spectrum obtained after Pronase-treatment of the MNP/•CuE-SOD1 radical adducts lacked the intensity required for any detailed hyperfine coupling analysis. Since the nitroso-based spin trap DBNBS also spin traps protein-centred radicals, often with a different specificity from that of MNP, the spin trapping experiments were repeated using DBNBS (Figure 4). No significant adduct formation was detected from the reaction between CuZn-SOD1 and H_2O_2 with or without added bicarbonate (Figure 4A and B), but an immobilized nitroxide radical adduct was detected in the reaction

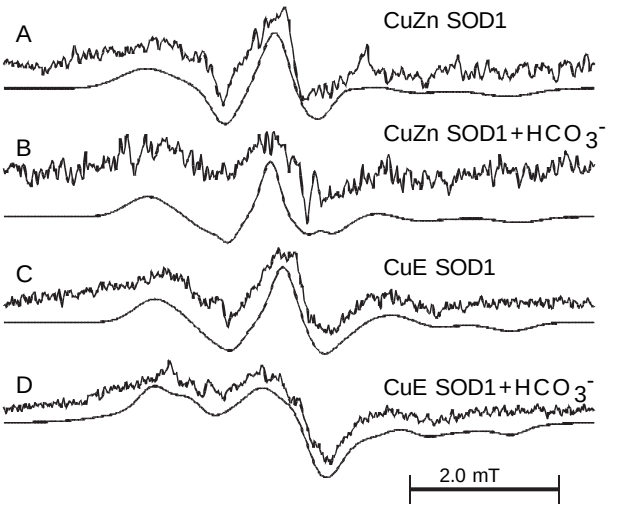

Figure 3. Powder pattern simulations of MNP/•SOD1 adducts. (A) Experimental spectrum from Figure 1A (CuZn SOD1+H_2O_2+MNP) and simulated spectrum (g_x = 2.001 72; g_y = 2.006 17; g_z = 2.004 93; a_x = 2.789 mT; a_y = 0.722 mT; a_z = 1.040 mT; linewidth peak to peak = 0.122 mT; linewidth perpendicular = 1.0942 mT). Averaging of the g-value and a^N values give an approximate isotropic g value of 2.0043 and a^N_{iso} = 1.52 mT. (B) Experimental spectrum from Figure 2A (CuZn SOD1+H_2O_2+HCO_3^-) and its simulation calculated assuming two species were present in the sample: species 1, 91% of total intensity (g_x = 2.002 06; g_y = 2.005 08; g_z = 2.006 60; a_x = 2.53 mT; a_y = 1.354 mT; a_z = 0.62 mT, giving g_{iso} = 2.0046 and a^N_{iso} = 1.50 mT); species 2, 9% of total intensity (g_x = 2.0037; g_y = 2.005 25; g_z = 2.007 34; a_x = 1.748 mT; a_y = 0.735 mT; a_z = 0.315 mT giving g_{iso} = 2.005 44 and a^N_{iso} = 1.50 mT). (C) Experimental spectrum from Figure 1F (CuE-SOD1+H_2O_2+MNP) and simulation calculated from the following parameters: g_x = 2.0025; g_y = 2.004 42; g_z = 2.006 14; a_x = 2.43 mT; a_y = 1.442 mT; a_z = 0.697 mT giving the approximate isotropic values g_{iso} = 2.004 36 and a^N_{iso} = 1.52 mT. (D) Experimental spectrum from Figure 2E (CuE-SOD1+H_2O_2+MNP+HCO_3^-) and its computer simulation calculated assuming two species: species 1, 8% of total intensity, g_x = 2.002 50; g_y = 2.004 48; g_z = 2.006 14; a_x = 2.43 mT; a_y = 1.44 mT; a_z = 0.700 mT, giving the isotropic values g_{iso} = 2.0043 and a^N_{iso} = 1.52 mT; species 2, 92% of total intensity, g_x = 2.002 87; g_y = 2.006 02; g_z = 2.007 04; a_x = 1.997 mT; a_y = 0.377 mT; a_z = 0.026 mT, giving the approximate isotropic values g_{iso} = 2.0053 and a^N_{iso} = 0.800 mT.

between CuE-SOD1 and H_2O_2 (Figure 4C). Pronase treatment of the DBNBS/•CuE-SOD1 adduct converted its EPR spectrum to an isotropic triplet (a^N = 1.37 mT) with additional unresolved hyperfine couplings (Figure 4D). In analogy to the corresponding MNP-trapping reaction, it was suspected that a histidinyl radical had been trapped. Authentic DBNBS/•histidine adducts were obtained from the reaction between histidine and the Fenton reagent ($Fe^{2+} + H_2O_2$) (Figure 4G). Two radical adducts were detected (Figure 4G), the first with a^N = 1.34 mT and unresolved additional hyperfine interactions and the second with a^N = 1.36 mT and additional hyperfine interactions with one nitrogen atom ($a^{N\beta}$ = 0.36 mT and one hydrogen atom (a^H = 0.72 mT), consistent with trapping the radical formed by the α-decarboxylation reaction of histidine. The former adduct could be well fit assuming partially resolved hyperfine interactions with two nitrogen atoms (see data in Table I) and the same parameters provided an excellent fit to the lineshapes of the EPR spectrum obtained from Pronase-treated DBNBS/•CuE-SOD1 (Figure 4D, 'simulation'). The EPR spectrum obtained from the CuE-SOD1/bicarbonate/H_2O_2/DBNBS system appeared to be a combination of a rotationally immobilized nitroxide and an isotropic nitroxide whose EPR spectrum was extremely similar to the spectrum obtained after Pronase-treatment of the DBNBS/•CuE-SOD1 adduct (Figure 4E). Indeed, after Pronase-treatment of the adduct(s), the resulting EPR spectrum was essentially indistinguishable from the spectrum obtained without (bi)carbonate, strongly suggesting trapping of a histidinyl radical (Figure 4F).

The hyperfine coupling data that could be extracted from the Pronase-treated MNP/•CuE-SOD1 radical formed in the reaction with (bi)carbonate were largely consistent with trapping a histidinyl radical (an apparent coupling to a nitrogen atom, a^N = 0.24 mT and probably an unresolved coupling with a hydrogen atom, $a^H \sim 0.09$ mT). The slight variation between the best fit for the nitroxide a^N (1.49 mT) and the value of a^N for authentic C-5-centred histidinyl radical (1.53 mT) could be accounted for in the uncertainty in the location of the highest field lines in the experimental spectrum. Simulation of the experimental spectrum using a value of $a^{N(NO)}$ = 1.53 mT resulted in only a slight decrease in the mathematical correlation value between the simulated and experimental spectra (r decreases from 0.63–0.61), supporting the probability of trapping a histidinyl radical.

CuZn-SOD1 reacts with peroxynitrite to form a protein-centred radical

Since peroxynitrite ($ONOO^-$) is an anionic peroxide as well as a potent nitrating and oxidizing agent, its proposed role in the neurotoxicity of CuE-SOD1 [23] might arise from free radical formation through the interaction of $ONOO^-$ with the active site copper ion. When tetramethylammonium peroxynitrite (this salt was used because its H_2O_2 contamination is minimal due to its direct synthesis excluding H_2O_2 [47]) was reacted with CuZn-SOD1, the resulting product had an immobilized nitroxide type EPR spectrum consistent with formation of a protein-centred free radical (Figure 5A). Pronase-treatment of the MNP-adduct formed in the CuZn-SOD1/$ONOO^-$ reaction resulted in the conversion of its EPR spectrum into a combination of an isotropic component ($a^N \sim 1.61$ mT; a^H = 0.11 mT (2H)) and an anisotropic component which accounted for the bulk of the intensity (Figure 5B). The isotropic component of that spectrum might have arisen from

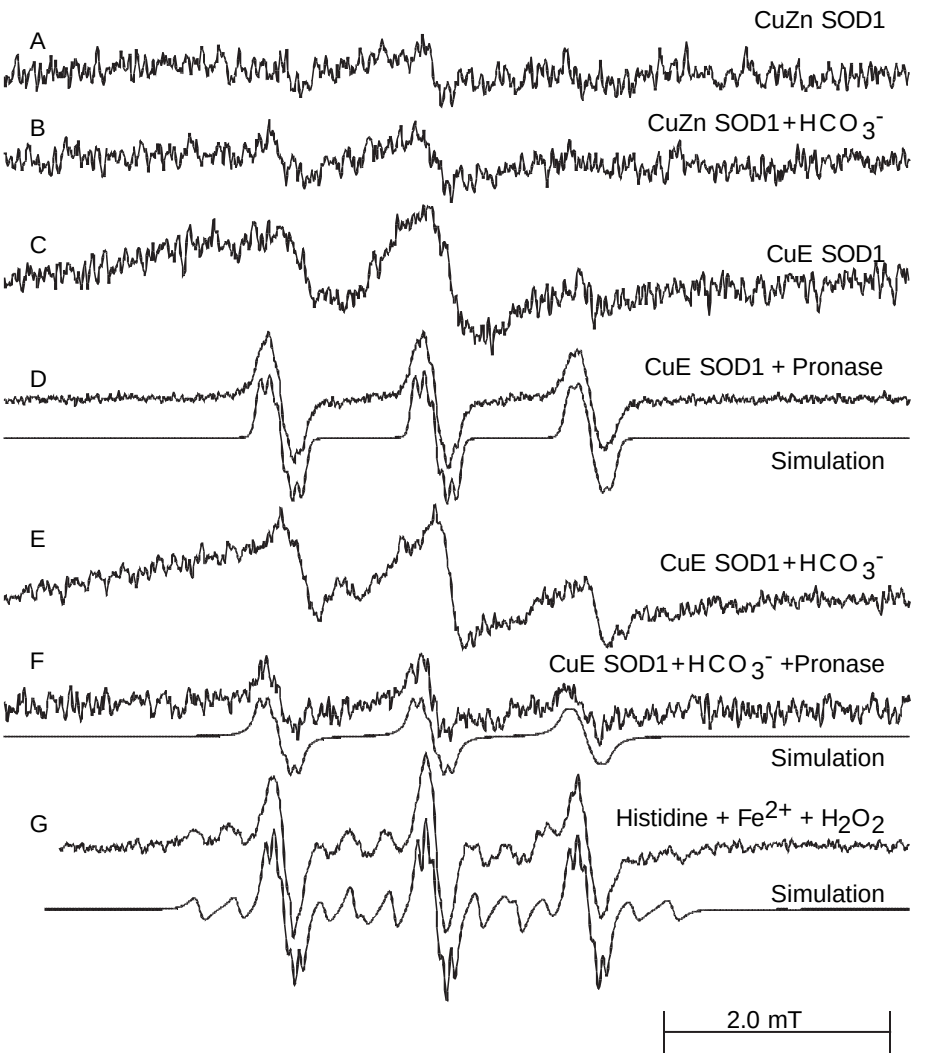

Figure 4. The free radicals formed in the CuE-H_2O_2 reaction are readily trapped by DBNBS. SOD1 (0.5 mM for spectra A–D, 0.25 mM for spectra E–F) was incubated with H_2O_2 (2.5 mM for spectra A–D; 1.25 mM for spectra E–F), DTPA (1 mM) and DBNBS (0.5 mM for spectra A–D; 0.25 mM for spectra E–F) for 5 min at room temperature before the experimental spectra were acquired. (A) CuZn SOD1+ H_2O_2 in phosphate buffer. (B) CuZn SOD1+H_2O_2 in bicarbonate buffer (25 mM, pH 7.4). (C) CuE SOD1+H_2O_2 in phosphate buffer (50 mM, pH 7.4). (D) The EPR spectrum obtained after incubation of a sample identical to the sample giving rise to Spectrum C with Pronase (10 mg/ml) for 5 min at room temperature; the spectrum shown is the second scan of the sample. The simulation of Spectrum D was calculated using the hyperfine coupling constants reported in Table I. (E) CuE SOD1 was incubated with H_2O_2 in bicarbonate buffer. The sample volume for this scan was 100 µl; 150 µl were used for the above experimental spectra. (F) The EPR spectrum obtained after treatment of the solution used to obtain Spectrum E with Pronase (10 mg/ml) for 5 min at room temperature. The computer simulation was calculated using the parameters reported in Table I. (G) The EPR spectrum obtained from a sample containing histidine (200 mM), DBNBS (1 mM), H_2O_2 (2 mM) and Fe^{2+} (1 mM). The computer simulation of the spectrum was obtained using the parameters reported in Table I including two different components. Experimental spectra A–C and E were obtained using the following instrument parameters: modulation amplitude, 2 G; scan time 335 s (8.0 mT scan); time constant, 0.67 s; three scans were added together to obtain the final spectra. Spectra D and F were acquired using the following instrument parameters: modulation amplitude, 0.1 mT; scan time 335 s (8.0 mT); time constant, 0.33 s., one scan.

a radical that resulted from the loss of a functional group on an amino acid residue, which would provide two equivalent hydrogen atoms, but no corresponding MNP adducts have been reported in the NIEHS spin trap data base, precluding a positive assignment of the adduct. All EPR signal was lost when a higher Pronase concentration was used (not shown). The anisotropic portion of the spectrum was very well fit by parameters that gave rise to an approximate isotropic a^N of 1.49 mT, which is typical of many carbon-centred MNP adducts and was therefore uninformative (Figure 5C). SOD1-centred adduct formation was prevented by inclusion of 5 mM cyanide, which prevents reactions of the active site Cu ion (Figure 5D). No MNP adduct was detected from the reaction between CuE-SOD1 and peroxynitrite (data not shown), suggesting that any adduct formed in that reaction was unstable inclusion of bicarbonate also prevented MNP adduct formation (data not shown). That result was not surprising since peroxynitrite is well known to react with (bi)carbonate to form an extremely unstable product that

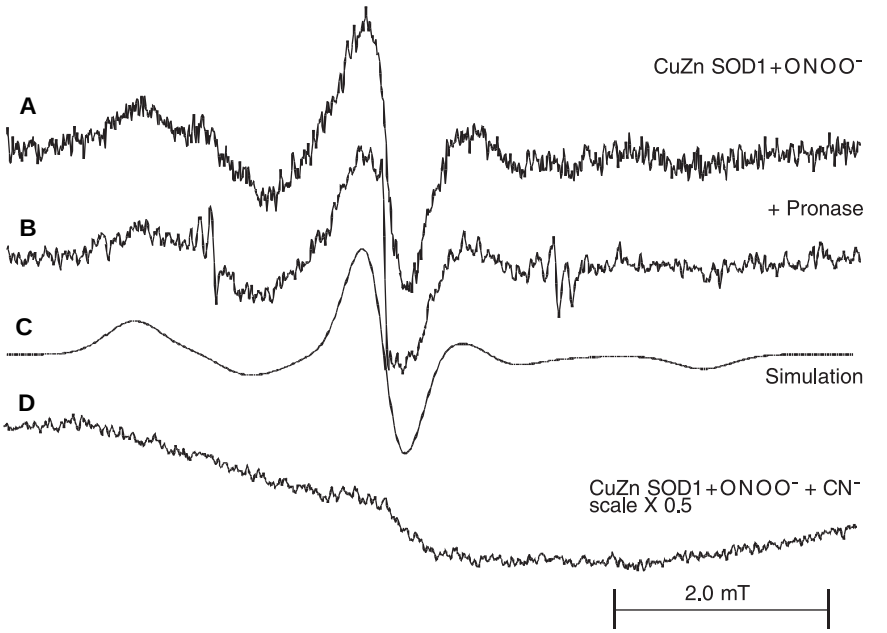

Figure 5. The reaction between CuZn SOD1 and peroxynitrite results in formation of an MNP-trappable free radical. SOD1 (0.5 mM) was incubated with MNP (10 mM), DTPA (1 mM) and tetramethylammonium peroxynitrite (2 mM) for 5 min at room temperature in either 50 mM sodium phosphate buffer, pH 7.4 or 25 mM bicarbonate buffer, pH 7.4, as indicated. (A) CuZn SOD1 was reacted with peroxynitrite in phosphate buffer. (B) The EPR spectrum obtained after treatment of a sample identical to the sample giving rise to Spectrum A with Pronase (20 mg/ml) for 5 min at room temperature. Note the superposition of istropic lines on either side of the central line of the anisotropic spectrum; those lines could be simulated with $a^N = 1.60$ mT and $a^H = 0.11$ mT (2H) (data not shown). (C) Powder pattern simulation of the anisotropic component of spectrum 6B, calculated using the following parameters: $g_x = 2.00506$, $g_y = 2.00877$, $g_z = 2.00705$; $a_x = 2.694$ mT; $a_y = 1.245$ mT, $a_z = 0.525$ mT (corresponding to the approximate isotropic values of $g_{iso} = 2.0066$, $a^N_{iso} = 1.488$ mT. (D) CuZn SOD1 was incubated with peroxynitrite as in Spectrum A in phosphate buffer containing NaCN (5 mM). All experimental spectra were obtained using the following instrument parameters: modulation amplitude, 0.1 mT; scan time 335 s (8.0 mT); time constant, 0.66 s and a single scan was collected in all cases.

rapidly decays into a variety of products [48]. Optical spectra of the CuZn-SOD1/peroxynitrite and CuE-SOD1/peroxynitrite products indicated a similar level of tyrosine nitration between the two samples (data not shown), indicating that the differences in free radical formation did not reflect differential reactivity of the peroxynitrite used in the two samples.

Discussion

The histidine C-5-centred radical is probably formed at His-118

The SOD1/•MNP EPR spectra obtained in the absence of (bi)carbonate (both CuZn-SOD1 and CuE-SOD1) indicated the trapping of radicals centred at two different atoms, C-2 and C-5, of the imidazole rings of histidine residues (Figures 1C and D; see Figure 6 for the structures of the radical adducts discussed in this study). Direct EPR studies have demonstrated that hydroxyl radical (similar to the initial oxidant formed in the SOD1/H_2O_2 reaction, see reaction 2, above) adds to the imidazole ring of histidine at C-2 and C-5 forming free radicals that are delocalized across the remaining atoms of the ring [49,50]. Addition of hydroxyl radical to C-2 of the imidazole ring of a histidine residue would form a radical that was trappable at C-5 and that could be converted to 2-oxohisitidine through an additional one electron oxidation. Since His-118 of bovine SOD1 is converted to 2-oxohistidine by H_2O_2-treatment of the protein [51], the radical trapped at C-5 of a histidine imidazole ring is probably centred on His-118 (see Figure 7). Likewise, addition of molecular oxygen to a radical centred at C-4 (also formed through the addition of hydroxyl radical at C-2) of a histidine imidazole ring would yield a peroxyl radical product that could readily decompose to form aspartic acid (see below). We have previously shown that both histidinyl radical (formed in the reaction between histidine and hydroxyl radical) and oxidized SOD1 react with molecular oxygen, presumably to form peroxyl radicals [41].

Histidine-61 may form the imidazole C-2-centred radical

The current data do not allow a direct assignment of the C-2-centred histidinyl radical. Since amino acid analysis of the bovine SOD1 protein after its reaction with a large excess of H_2O_2 indicated the loss of two histidine residues and one proline residue (accompanied by gains of one aspartate, one glutamate, and one 2-oxohistidine residue [51]), we expect that a second histidine residue is oxidized (as opposed to the formation of two different radicals on the same histidine). Previous reports,

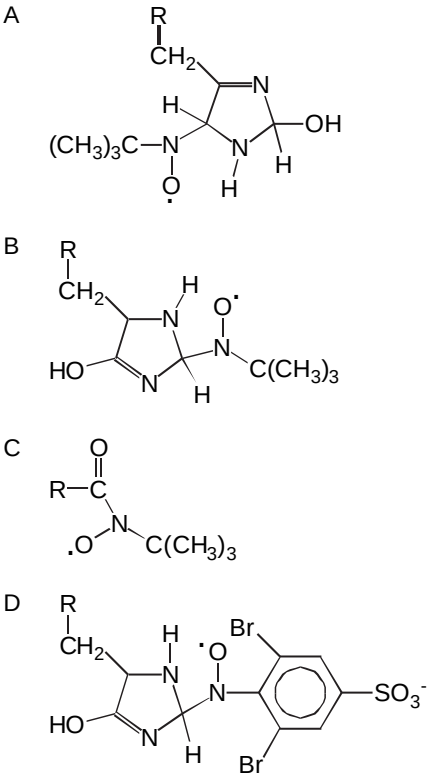

Figure 6. Structures of the radical adducts discussed in this study. (A) The MNP adduct centred on C-5 of the imidazole ring of a histidine residue formed through the addition of hydroxyl radical to C-2 of the ring. (B) The MNP adduct centred on C-2 of the imidazole ring of a histidine residue formed through the addition of hydroxyl radical to C-5 of the ring. (C) The MNP adduct on a carbonyl carbon formed in the carbonate radical oxidation of an amino acid side chain. (D) The DBNBS adduct of a radical centred on C-2 of the imidazole ring of a histidine residue.

along with the active site structure of the bovine SOD1 protein, support the oxidation of His-61. Treatment of human SOD1 protein with a large excess of hydrogen peroxide resulted in the fragmentation of the protein at the bond between His-63 and Pro-62, which correspond to His-61 and Pro-60 of bovine SOD1 [52]. A peroxyl radical centred on the imidazole ring of His-61 would be in the ideal position to oxidize the amide bond connecting Pro-60 to His-61 (see Figure 7). Oxidation of that bond would likely cause fragmentation of the backbone at that site [52] and also the site-specific fragmentation detected by Western blotting in bovine SOD1 oxidized by H_2O_2 [39]. Backbone fragmentation was not detected under our experimental conditions (data not shown), suggesting that additional oxidizing equivalents may be necessary for that reaction. Backbone oxidation between His-61 and Pro-60 would also be consistent with the conversion of that Proline residue to a glutamate [51]. Damage to the imidazole ring of His-61, a ligand of both the zinc and copper ions, is consistent with the reported loss of zinc affinity in H_2O_2-treated CuE-SOD1 protein [42] and with the

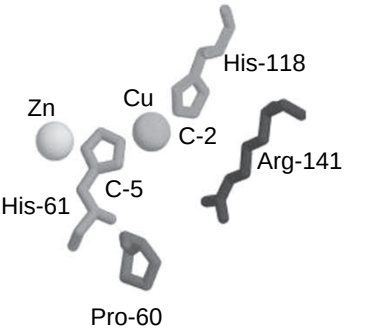

Figure 7. Structure of the active site of bovine SOD1 and the amino acid residues likely oxidized in the self-peroxidation reaction. Residues 61 and 118 are histidine residues that ligand the copper ion and, in the case of His-61, the zinc ion and have been proposed to be the sites of histidinyl radical formation. Proline-60 is shown because the amide bond between the corresponding residues in human SOD1 has been shown to be broken in the reaction between that protein and excess hydrogen peroxide [52]. Arginine-141 is the positively charged residue located at the entrance of the substrate binding site, such that the face of the copper ion facing the arginine residue is the likely site of the initial oxidant formation when SOD1 reacts with hydrogen peroxide. The structure was taken from the 1CB4 crystal structure of bovine SOD1 protein [56] and the image was generated using the Rasmol program.

peroxide-dependent loss of copper [39,53] from the protein. Furthermore, like C-2 of the imidazole ring of His-118, C-5 of His-61 is adjacent to the copper ion and facing the entrance of the substrate-binding pocket of SOD1, making both of those atoms ideal targets for the addition of hydroxyl radical formed on that face of the copper ion (Figure 7). We therefore propose that the C-2 centred histidinyl radical is formed on His-61.

Removal of the active site zinc increases accessibility of the active site

In the absence of added bicarbonate, the removal of the active site zinc ion had no effect on the MNP-trappable free radicals formed when SOD1 reacted with H_2O_2 (Figure 1). However, the removal of the active site zinc ion did result in detection of a DBNBS-trappable histidinyl radical that was probably centred on C-2 of the imidazole ring (and therefore was probably located on His-61 as discussed above) (Figures 3 and 6D). Since the reactive nitroso group on DBNBS is more sterically hindered than the corresponding group on MNP, the DBNBS trapping data suggests that the removal of the active site zinc ion caused increased accessibility in the active site of the protein. That conclusion is supported both by crystallography studies indicating that the zinc ion anchors the electrostatic and zinc-binding loops of the protein [54] and by a spectroscopic study indicating decreased β-sheet content in CuE-SOD1 compared to CuZn-SOD1 [55].

Carbonate radical oxidizes a unique site on CuE-SOD1

Previous studies have strongly suggested that aqueous CO_2 (which is in equilibrium with bicarbonate anion) is oxidized by the initially-formed oxidant in the SOD1-H_2O_2 reaction (see reactions 1–5, above) to form the carbonate radical anion [33–40]. The product carbonate radical is an obligate intermediate in the oxidation of small molecule probes of the SOD1 pseudoperoxidase reaction [34,35,40]. The minimal effects of added bicarbonate on the self-peroxidation of CuZn-SOD1 (Figures 2A and B) were consistent with a previous report indicating oxidation of a histidine residue in bovine SOD1 by carbonate radical [38]. In the absence of the active site zinc ion, however, carbonate radical oxidized a unique target on the SOD1 protein that could not be unambiguously identified from the data (Figures 2 and 3). The approximate value of the nitroxide nitrogen hyperfine coupling constant ($a^N \approx 0.8$ mT) indicated that the radical adduct was centred on a carbonyl carbon (Figure 6C). Such a radical adduct could be formed upon the free radical mediated fragmentation of the backbone of the protein or from the oxidation of an amino acid residue with a carboxylate or carboxamide side chain. Separation of the SOD1 products of the reaction on an SDS-polyacrylamide gel provided no evidence that fragmentation was the major product of the reaction (data not shown), suggesting the trapped radical arose from the oxidation of an amino acid side chain. One such possible target would be the side chain of Asp-80, which is one of the ligands of the zinc ion, but no experimental data is available to support that speculation. Damage to the side chain of Asp-80 would be consistent with the reported loss of zinc affinity in peroxide-treated CuE-SOD1 [42].

SOD1 peroxidation and neurodegeneration

A recent study found the accumulation of oxidized SOD1 protein in human brains from victims of Parkinson's Disease and Alzheimer's disease [12]. The self-peroxidation reaction of SOD1 ultimately results in the formation of protein carbonyls (such as 2-oxohistidine) that have been detected in those diseases. Zinc-deficient SOD1 protein has also previously been shown to be toxic to motor neurons exposed to nitric oxide, suggesting that reactions of the CuE-form of the protein are toxic [23]. Our results clearly demonstrated that, in the presence of (bi)carbonate, CuE-SOD1 protein forms additional and different protein-centred free radicals when reacting with H_2O_2 compared to the CuZn form of the protein. Some of those radicals (centred on a carbonyl carbon) are likely much more reactive than the histidinyl radicals formed on CuZn-SOD1. Treatment of *Xenopus* oocytes that expressed both a mutant SOD1 protein and a glutamate transporter that is important in excitotoxic damage to neurons with H_2O_2 resulted in the specific loss of activity of the glutatmate transporter [11], supporting a role for the SOD1-H_2O_2 reaction in mutant SOD1-linked ALS. A role for H_2O_2 in the pathogenesis of the disease was further supported by the protective effects of putrescein-labelled catalase upon mutant SOD1-expressing mice [10]. The present results also suggest increased escape of the carbonate radical from the active site of the zinc-deficient protein, even though the relatively oxidizable surface tyrosine residue was not targeted in the reaction.

It has been previously proposed that the experimentally observed neurotoxicity of the zinc-deficient SOD1 protein involved the reactions of peroxynitrite since increased NO concentrations were found to induce neurotoxicity [23]. Our results clearly indicate that, in addition to tyrosine nitrating reactions, peroxynitrite can also act as an inorganic peroxide to activate the peroxidase activity of the SOD1 protein. The peroxynitrite-dependent self-peroxidation reaction caused radical formation that was consistent with the removal of the functional group on the side chain of an amino acid residue rather than oxidizing a side chain (a radical was trapped that had an EPR signal consistent with trapping on a methylene carbon) suggesting an entirely different active site oxidant is formed in the SOD1-peroxynitrite reaction. However, in those reactions the CuZn-SOD1 protein was much more active than was the zinc-deficient form of the protein, suggesting that the peroxynitrite-activated peroxidase reaction is unlikely to be the cause of the neurotoxicity of zinc-deficient SOD1.

Acknowledgements

This research was supported, in part, by grants from the West Virginia University Research Corporation and from the ALS Association.

References

[1] Rosen DR, Siddique T, Patterson D, Figlewicz DA, Sapp P, Hentati A, Donaldson D, Goto J, O'Regan JP, Deng HX, Rahmani Z, Krizus A, McKenna-Yasek D, Cayabyab A, Gaston SM, Berger R, Tanzi RE, Halperin JJ, Herzfeldt B, Van den Bergh R, Hung WY, Bird T, Deng G, Mulder DW, Smyth C, Laing NG, Soriano E, Pericak-Vance MA, Haines J, Rouleau GA, Gusella JS, Horvitz HR, Brown RH Jr. Mutations in Cu/Zn superoxide dismutase gene are associated with familial amyotrophic lateral sclerosis. Nature 1993;362: 59–62.

[2] Deng HX, Hentati A, Tainer JA, Iqbal Z, Cayabyab A, Hung WY, Getzoff ED, Hu P, Herzfeldt B, Roos RP, Warner C, Deng G, Soriano E, Smyth C, Parge HE, Ahmed A, Roses AD, Hallewell RA, Pericak-Vance MA, Siddique T. Amotrophic lateral sclerosis and structural defects in Cu,Zn superoxide dismutase. Science 1993;261: 1047–1051.

[3] Gurney ME, Pu H, Chiu AY, Dal Canto MC, Polchow CY, Alexander DD, Caliendo J, Hentati A, Kwon YW, Deng HX, Chen W, Zhai P, Sufit RL, Siddique T. Motor neuron degeneration in mice that express a human Cu,Zn superoxide dismutase mutation. Science 1994;264:1772–1775.

[4] Ferrante RJ, Shinobu LA, Schulz JB, Matthews RT, Thomas CT, Kowall NW, Gurney ME, Beal MF. Increased 3-nitrotyrosine and oxidative damage in mice with a human copper/zinc superoxide dismutase mutation. Ann Neurol 1997;42:326–334.

[5] Hall ED, Andrus PK, Oostveen JA, Fleck TJ, Gurney ME. Relationship of oxygen radical-induced lipid peroxidative damage to disease onset and progression in a transgenic model of familial ALS. J Neurosci Res 1998;53:66–77.

[6] Bogdanov MB, Ramos LE, Xu Z, Beal MF. Elevated 'hydroxyl radical' generation *in vivo* in an animal model of amyotrophic lateral sclerosis. J Neurochem 1998;71:1321–1324.

[7] Liu R, Althaus JS, Ellerbrock BR, Becker DA, Gurney ME. Enhanced oxygen radical production in a transgenic mouse model of familial amyotrophic lateral sclerosis. Ann Neurol 1998;44:763–770.

[8] Said Ahmed M, Hung WY, Zu JS, Hockberger P, Siddique T. Increased reactive oxygen species in familial amyotrophic lateral sclerosis with mutations in SOD1. J Neurol Sci 2000;176:88–94.

[9] Nagano S, Ogawa Y, Yanagiahara T, Sakoda S. Benefit of a combined treatment with trientine and ascorbate in familial amyotrophic lateral sclerosis model mice. Neurosci Lett 1999;265:159–162.

[10] Reinholz MM, Merkle CM, Poduslo JF. Therapeutic benefits of putrescine-modified catalase in a transgenic mouse model of familial amyotrophic lateral sclerosis. Exp Neurol 1999;159:204–216.

[11] Trotti D, Rolfs A, Danbolt NC, Brown RH Jr, Hediger MA. SOD1 mutants linked to amyotrophic lateral sclerosis selectively inactivate a glial glutamate transporter. Nature Neurosci 1999;2:427–433.

[12] Choi J, Rees HD, Weintraub ST, Levey AI, Chin LS, Li L. Oxidative modifications and aggregation of Cu,Zn-superoxide dismutase associated with Alzheimer and Parkinson diseases. J Biol Chem 2005;280:11648–11655.

[13] Moreira PI, Honda K, Liu Q, Santos MS, Oliveira CR, Aliev G, Nunomura A, Zhu X, Smith MA, Perry G. Oxidative stress: the old enemy in Alzheimer's disease pathophysiology. Curr Alzheimer Res 2005;2:403–408.

[14] Fasano M, Bergamasco B, Lopiano L. Modifications of the iron-neuromelanin system in Parkinson's disease. J Neurochem 2006;96:906–916.

[15] Tabner BJ, El-Agnaf OMA, Turnbull S, German MJ, Paleologou KE, Hayashi Y, Cooper LJ, Fullwood NJ, Allsop D. Hydrogen peroxide is generated during the very early stages of aggregation of the amyloid peptides implicated in Alzheimer disease and familial british dementia. J Biol Chem 2005;280:35789–35792.

[16] Santos MJ, Quintanilla RA, Toro A, Grandy R, Dinamarca MC, Godoy JA, Inestrosa NC. Peroxisomal proliferation protects from β-amyloid neurodegeneration. J Biol Chem 2005;280:41057–41068.

[17] Tiwari A, Xu Z, Hayward LJ. Aberrantly increased hydrophobicity shared by mutants of Cu,Zn-superoxide dismutase in familial amyotrophic lateral sclerosis. J Biol Chem 2005;280:29771–29779.

[18] Elam JS, Taylor AB, Strange R, Antonyuk S, Doucette PA, Rodriguez JA, Hasnain SS, Hayward LJ, Valentine JS, Yeates TO, Hart PJ. Amyloid-like filaments and water-filled nanotubes formed by SOD1 mutant proteins linked to familial ALS. Nature Struct Biol 2003;10:461–467.

[19] Vijayvergiya C, Beal MF, Buck J, Manfredi G. Mutant superoxide dismutase 1 forms aggregates in the brain mitochondrial matrix of amyotrophic lateral sclerosis mice. J Neurosci 2005;25:2463–2470.

[20] Crow JP, Sampson JB, Zhuang Y, Thompson JA, Beckman JS. Decreased zinc affinity of amyotrophic lateral sclerosis-associated superoxide dismutase mutants leads to enhanced catalysis of tyrosine nitration by peroxynitrite. J Neurochem 1997;69:1936–1944.

[21] Goto JJ, Zhu H, Sanchez RJ, Nersissian A, Gralla EB, Valentine JS, Cabelli DE. Loss of *in vitro* metal ion binding specificity in mutant copper-zinc superoxide dismutases associated with familial amyotrophic lateral sclerosis. J Biol Chem 2000;275:1007–1014.

[22] Hayward LJ, Rodriguez JA, Kim JW, Tiwari A, Goto JJ, Cabelli DE, Valentine JS, Brown RH Jr. Decreased metallation and activity in subsets of mutant superoxide dismutases associated with familial amyotrophic lateral sclerosis. J Biol Chem 2002;277:15923–15931.

[23] Estevez AG, Crow JP, Sampson JB, Reiter C, Zhuang Y, Richardson GJ, Tarpey MM, Barbeito L, Beckman JS. Induction of nitric oxide-dependent apoptosis in motor neurons by zinc-deficient superoxide dismutase. Science 1999;286:2498–2500.

[24] Bruijn LI, Houseweart MK, Kato S, Anderson KL, Anderson SD, Ohama E, Reaume AG, Scott RW, Cleveland DW. Aggregation and motor neuron toxicity of an ALS-linked SOD1 mutant independent from wild type SOD1. Science 1998;281:1851–1854.

[25] Okado-Matsumoto A, Myint T, Fujii J, Taniguchi N. Gain in functions of mutant Cu,Zn-superoxide dismutases as a causative factor in familial amyotrophic lateral sclerosis: less reactive oxidant formation but high spontaneous aggregation and precipitation. Free Radic Res 2000;33:65–73.

[26] Shinder GA, Lacourse MC, Minotti S, Durham HD. Mutant Cu/Zn superoxide dismutase proteins have altered solubility and interact with heat shock/stress proteins in models of amyotrophic lateral sclerosis. J Biol Chem 2001;276:12791–12796.

[27] Brown RH Jr. SOD1 aggregates in ALS: cause, correlate, or consequence? Nat Med 1998;4:1362–1364.

[28] Hodgson EK, Fridovich I. The interaction of bovine erythrocyte superoxide dismutase with hydrogen peroxide: inactivation of the enzyme. Biochemistry 1975;14:5294–5299.

[29] Hodgson EK, Fridovich I. The interaction of bovine erythrocyte superoxide dismutase with hydrogen peroxide: chemiluminescence and peroxidation. Biochemistry 1975;14:5299–5303.

[30] Yim MB, Kang JH, Yim HS, Kwak HS, Chock PB, Stadtman ER. A gain-of-function of an amyotrophic lateral sclerosis-associated Cu,Zn-superoxide dismutase mutant: an enhancement of free radical formation due to a decrease in K_M for hydrogen peroxide. Proc Natl Acad Sci USA 1996;93:5709–5714.

[31] Singh RJ, Karoui H, Gunther MR, Beckman JS, Mason RP, Kalyanaraman B. Reexamination of the mechanism of hydroxyl radical adducts formed from the reaction between familial amyotrophic lateral sclerosis-associated Cu,Zn superoxide dismutase mutants and H_2O_2. Proc Natl Acad Sci USA 1998;95:6675–6680.

[32] Wiedeau-Pazos M, Goto JJ, Rabizadeh S, Gralla EB, Roe JA, Lee MK, Valentine JS, Bredesen DE. Altered reactivity of superoxide dismutase in familial amyotrophic lateral sclerosis. Science 1996;271:515–518.

[33] Sankarapandi S, Zweier JL. Bicarbonate is required for the peroxidase function of Cu, Zn-superoxide dismutase at physiological pH. J Biol Chem 1999;274:1226–1232.

[34] Zhang H, Joseph J, Felix C, Kalyanaraman B. Bicarbonate enhances the hydroxylation, nitration, and peroxidation reactions catalyzed by copper, zinc superoxide dismutase. Intermediacy of carbonate anion radical. J Biol Chem 2000;275:14038–14045.

[35] Zhang H, Andrekopoulos C, Joseph J, Chandran K, Karoui H, Crow JP, Kalyanaraman B. Bicarbonate-dependent peroxidase activity of human Cu,Zn-superoxide dismutase induces covalent aggregation of protein: intermediacy of tryptophan-derived oxidation products. J Biol Chem 2003;278:24078–24089.

[36] Karunakaran C, Zhang H, Crow JP, Antholine WA, Kalyanaraman B. Direct probing of copper active site and free radical formed during bicarbonate-dependent peroxidase activity of bovine and human copper, zinc-superoxide dismutases. Low-temperature electron paramagnetic resonance and electron nuclear double resonance studies. J Biol Chem 2004;279:32534–32540.

[37] Andrekopoulos C, Zhang H, Joseph J, Kalivendi S, Kalyanaraman B. Bicarbonate enhances alpha-synuclein oligomerization and nitration: intermediacy of carbonate radical anion and nitrogen dioxide radical. Biochem J 2004;378:435–447.

[38] Bonini MG, Fernandes DC, Augusto O. Albumin oxidation to diverse radicals by the peroxidase activity of Cu,Zn-superoxide dismutase in the presence of bicarbonate or nitrite: diffusible radicals produce cysteinyl and solvent-exposed and -unexposed tyrosyl radicals. Biochemistry 2004;43:344–351.

[39] Ramirez DC, Gomez Mejiba SE, Mason RP. Mechanism of hydrogen peroxide-induced Cu,Zn-superoxide dismutase-centered radical formation as explored by immuno-spin trapping: the role of copper- and carbonate radical anion-mediated oxidations. Free Radic Biol Med 2005;38:201–214.

[40] Liochev SI, Fridovich I. CO_2, not HCO_3^-, facilitates oxidations by Cu,Zn superoxide dismutase plus H_2O_2. Proc Natl Acad Sci USA 2004;101:743–744.

[41] Gunther MR, Peters JA, Sivaneri MK. Histidinyl radical formation in the self-peroxidation reaction of bovine copper-zinc superoxide dismutase. J Biol Chem 2002;277:9160–9166.

[42] Sampson JB, Beckman JS. Hydrogen peroxide damages the zinc-binding site of zinc-deficient Cu,Zn superoxide dismutase. Arch Biochem Biophys 2001;392:8–13.

[43] Crow JP, Ishciropoulos H. Detection and quantitation of nitrotyrosine residues in proteins: *in vivo* marker of peroxynitrite. Methods Enzymol 1996;269:185–194.

[44] Rustgi SN, Riesz P. An ESR and spin-trapping study of the reactions of the SO_4^- radical with protein and nucleic acid constituents. Int J Radiat Biol 1978;34:301–316.

[45] Mottley C, Robinson RE, Mason RP. Free radical formation in the oxidation of malondialdehyde and acetylacetone by peroxidase enzymes. Arch Biochem Biophys 1991;289:153–160.

[46] Rustgi SN, Riesz P. Free radicals in UV irradiated aqueous solutions of substituted amides. An ESR and spin-trapping study. Int J Radiat Biol 1978;34:149–163.

[47] Bohle DS, Hansert B, Paulson SC, Smith BD. Biomimetic synthesis of the putative cytotoxin peroxynitrite, $ONOO^-$, and its characterization as a tetramethylammonium salt. J Am Chem Soc 1994;116:7423–7424.

[48] Squadrito GL, Pryor WA. Oxidative chemistry of nitric oxide: the roles of superoxide, peroxynitrite, and carbon dioxide. Free Radic Biol Med 1998;25:392–403.

[49] Lassmann G, Eriksson LA, Himo F, Lendzian F, Lubitz W. Electronic structure of a transient histidine radical in liquid aqueous solution: EPR continuous-flow studies and density functional calculations. J Phys Chem A 1999;103:1283–1290.

[50] Lassmann G, Eriksson LA, Lendzian F, Lubitz W. Structure of a transient neutral histidine radical in solution: EPR continuous-flow studies in a Ti^{3+}/EDTA—Fenton system and density functional calculations. J Phys Chem A 2000;104:9144–9152.

[51] Uchida K, Kawakishi S. Identification of oxidized histidine generated at the active site of Cu,Zn-superoxide dismutase exposed to H_2O_2. J Biol Chem 1994;269:2405–2410.

[52] Ookawara T, Kawamura N, Kitagawa Y, Taniguchi N. Site-specific and random fragmentation of Cu,Zn-superoxide dismutase by glycation reaction. Implication of reactive oxygen species. J Biol Chem 1992;267:18505–18510.

[53] Sato K, Akaike T, Kohno M, Ando M, Maeda H. Hydroxyl radical production by H_2O_2 plus Cu,Zn-superoxide dismutase reflects the activity of free copper released from the oxidatively damaged enzyme. J Biol Chem 1992;267:25371–25377.

[54] Strange RW, Antonyuk S, Hough MA, Doucette PA, Rodriguez JA, Hart PJ, Hayward LJ, Valentine JS, Hasnain SS. The structure of holo and metal-deficient wild-type human Cu, Zn superoxide dismutase and its relevance to familial amyotrophic lateral sclerosis. J Mol Biol 2003;328:877–891.

[55] Sun WY, Fang JL, Cheng M, Xia PY, Tang WX. Secondary structure dependent upon metal ions of copper, zinc superoxide dismutase investigated by fourier transform IR spectroscopy. Biopolymers 1997;42:297–303.

[56] Hough MA, Hasnain SS. Crystallographic structures of bovine copper-zinc superoxide dismutase reveal asymmetry in two subunits: functionally important three and five coordinate copper sites captured in the same crystal. J Mol Biol 1999;287:579–592.